



Competition between green and infrared emission in Er:YLiF₄ upconversion lasers

Octavian Toma^{*}, Serban Georgescu

National Institute for Laser, Plasma and Radiation Physics, Solid-State Quantum Electronics Laboratory, 409 Atomistilor Street, 077125, Magurele, Jud. Ilfov, Romania

ARTICLE INFO

Article history:

Received 28 June 2010

Accepted 24 August 2010

Keywords:

Upconversion laser

Erbium

Dual-wavelength laser

ABSTRACT

The competition between two laser transitions in Er:YLiF₄ ($^4S_{3/2} \rightarrow ^4I_{15/2}$ at 551 nm and $^4S_{3/2} \rightarrow ^4I_{13/2}$ at 850 nm) is studied using a model based on rate equations. The laser emission is pumped by upconversion at 795 nm; for comparison, we also discuss upconversion pumping by another mechanism, at 970 nm. The conditions that favor laser emission in various regimes on these two transitions are found.

© 2010 Elsevier B.V. All rights reserved.

1. Introduction

The upconversion-pumped lasers are promising sources of visible coherent radiation, with possible applications in display technology, spectroscopy, biology and imaging. Among the active ions used in these lasers, Er³⁺ is one of the most investigated, due to its multitude of resonances between various transitions. The most interesting laser transition of Er³⁺ is $^4S_{3/2} \rightarrow ^4I_{15/2}$, which yields radiation in green (around 550 nm). Transition $^4S_{3/2} \rightarrow ^4I_{13/2}$, with emission around 850 nm, was also used to obtain visible radiation in blue (425 nm), by intracavity frequency doubling [1]. Parasitic emission on this transition was also observed accompanying emission on transition $^4S_{3/2} \rightarrow ^4I_{15/2}$ [2–4]. For the design of an efficient laser system on any or both of these transitions, it is therefore important to know the conditions that would lead to laser emission on any of them.

The dual-wavelength lasers are of great interest at present [5–8] due to their various applications (displays, medicine, holography, and laser spectroscopy). Besides the dual-wavelength lasers based on Nd³⁺, upconversion-pumped lasers with emission at two wavelengths were also demonstrated [9,10]; they also found various applications and their complexity can lead to interesting dynamics [10].

In a series of papers [11–13], we have studied the influence of excited-state reabsorption losses on the green laser emission on transition $^4S_{3/2} \rightarrow ^4I_{15/2}$ pumped by various mechanisms. In this work, we address the competition between the laser transitions $^4S_{3/2} \rightarrow ^4I_{15/2}$ and $^4S_{3/2} \rightarrow ^4I_{13/2}$. A possible application of an Er:YLF laser with simultaneous emission on both these transitions could be for simultaneous generation of visible green and blue (425 nm) radiation. This

would imply only frequency doubling of the 850 nm radiation, which can be accomplished in a simple set-up. Thereby, problems like the low power level or the set-up complexity observed in the previous attempts to obtain multiple-wavelength-emitting lasers in visible based on two-wavelength Nd lasers could be overcome [5,8].

The rate-equation model used in the previous works [12,13] was extended to include laser emission at 850 nm; the active medium investigated is Er(1%):YLiF₄ (Er:YLF), a crystal with low-energy phonons that yielded good performances in upconversion lasers. The low Er concentration of 1 at.% was chosen because it represents the usual compromise in room-temperature experiments [1,3,4] between a large concentration that would increase the influence of the cross-relaxation ($^4S_{3/2}, ^4I_{15/2} \rightarrow ^4I_{9/2}, ^4I_{13/2}$) that depletes the initial laser level $^4S_{3/2}$, and a small concentration that would lead to inefficient absorption of pump radiation in the active medium. However, the calculations performed in this work can be used to predict the behavior of any other erbium laser on these transitions pumped by the same upconversion mechanisms.

The transition $^4S_{3/2} \rightarrow ^4I_{13/2}$ is self-saturated, due to the lifetime of the final laser level being longer than the lifetime of the initial one. The best experimental results on this transition at room temperature were therefore obtained [1,14–17] for pump mechanisms using the final laser level $^4I_{13/2}$ as the intermediate pump level, the pump being used to deplete it and avoid self-saturation. Such a mechanism encourages the competition between the two laser transitions in discussion. One such pump mechanism, consisting of ground-state absorption (GSA) $^4I_{15/2} \rightarrow ^4I_{9/2}$ at 795 nm, followed by non-radiative decay to $^4I_{13/2}$ and excited-state absorption (ESA) [b] $^4I_{13/2} \rightarrow ^2H_{11/2}$ (see Fig. 1), is investigated here. For comparison, we also discuss another pump mechanism, that yielded the lowest emission threshold for the transition $^4S_{3/2} \rightarrow ^4I_{15/2}$ in our previous calculations [13]: GSA $^4I_{15/2} \rightarrow ^4I_{11/2}$ at 970 nm, followed by ESA [d] (see Fig. 1) at the same wavelength on the transition $^4I_{11/2} \rightarrow ^4F_{7/2}$ and non-radiative decay to thermalized levels ($^4S_{3/2}, ^2H_{11/2}$).

^{*} Corresponding author.

E-mail address: octavian.toma@inflpr.ro (O. Toma).

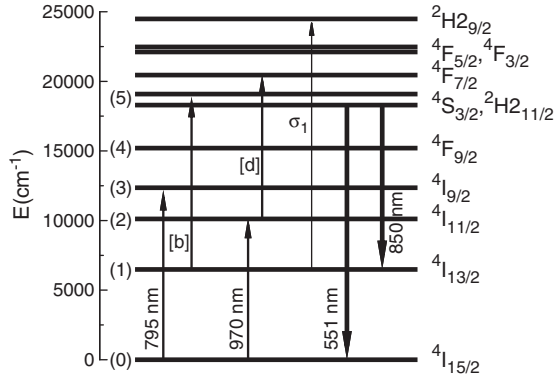


Fig. 1. Energy level scheme of $\text{Er}^{3+}:\text{YLF}$. The pump mechanisms of ${}^4\text{S}_{3/2}$ for pumping at 795 nm and 970 nm are represented together with the laser transitions and the ESR process at 551 nm.

2. Mathematical model

The mathematical model used here takes into account the absorption and emission processes represented in Fig. 1: the two pump mechanisms mentioned above (with the ESA transitions labeled with [b], respectively [d]), and the two laser transitions: ${}^4\text{S}_{3/2}$ (Stark level 2) \rightarrow ${}^4\text{I}_{15/2}$ (Stark level 8) and ${}^4\text{S}_{3/2}$ (Stark level 2) \rightarrow ${}^4\text{I}_{13/2}$ (Stark level 7); also included in our model is the excited-state reabsorption (ESR) of laser radiation at 551 nm on the transition ${}^4\text{I}_{13/2} \rightarrow {}^2\text{H}_{29/2}$ (of cross-section σ_1). A continuously pumped monolithic Er:YLF laser with spatial uniformity of the pump radiation inside the active medium was considered.

The rate equations system including these processes is the following:

$$\begin{aligned}
 \frac{dN_1}{dt} &= -\frac{N_1}{T_1} + \beta_{21}\frac{N_2}{T_2} + \beta_{31}\frac{N_3}{T_3} + \beta_{41}\frac{N_4}{T_4} \\
 &\quad + \beta_{51}\frac{N_5}{T_5} - \sigma_b\phi_2N_1 - \sigma_1N_1\varphi_G \\
 &\quad + \sigma_{51}(f_{52}N_5 - f_{17}N_1)\varphi_{IR} \\
 \frac{dN_2}{dt} &= -\frac{N_2}{T_2} + \beta_{32}\frac{N_3}{T_3} + \beta_{42}\frac{N_4}{T_4} + \beta_{52}\frac{N_5}{T_5} \\
 &\quad + \sigma_{04}\phi_4N_0 - \sigma_d\phi_4N_2 \\
 \frac{dN_3}{dt} &= -\frac{N_3}{T_3} + \beta_{43}\frac{N_4}{T_4} + \beta_{53}\frac{N_5}{T_5} + \sigma_{02}\phi_2N_0 \\
 \frac{dN_4}{dt} &= -\frac{N_4}{T_4} + \beta_{54}\frac{N_5}{T_5} \\
 \frac{dN_5}{dt} &= -\frac{N_5}{T_5} - \sigma_{50}(f_{52}N_5 - f_{08}N_0)\varphi_G \\
 &\quad + \sigma_b\phi_2N_1 + \sigma_d\phi_4N_2 + \sigma_1N_1\varphi_G \\
 &\quad - \sigma_{51}(f_{52}N_5 - f_{17}N_1)\varphi_{IR} \\
 \frac{d\varphi_G}{dt} &= v_G[\sigma_{50}(f_{52}N_5 - f_{08}N_0) - \sigma_1N_1 - \rho_G]\varphi_G + k_G\frac{N_5}{T_5} \\
 \frac{d\varphi_{IR}}{dt} &= v_{IR}[\sigma_{51}(f_{52}N_5 - f_{17}N_1) - \rho_{IR}]\varphi_{IR} + k_{IR}\frac{N_5}{T_5} \\
 N_t &= N_0 + N_1 + N_2 + N_3 + N_4 + N_5
 \end{aligned} \tag{1}$$

where N_i represents the populations of the Er^{3+} energy levels ${}^4\text{I}_{15/2}$, ${}^4\text{I}_{13/2}$, ${}^4\text{I}_{11/2}$, ${}^4\text{I}_{9/2}$, ${}^4\text{F}_{9/2}$ and ${}^4\text{S}_{3/2}$ thermalized with ${}^2\text{H}_{211/2}$ (numbered 0 to 5, see Fig. 1), while T_i represents the lifetimes of the first five excited levels and β_{ij} represents the branching ratios of transitions $i \rightarrow j$ between these levels. The laser photon flux was denoted by φ_G for the green emission (transition ${}^4\text{S}_{3/2} \rightarrow {}^4\text{I}_{15/2}$) and by φ_{IR} for the infrared emission (transition ${}^4\text{S}_{3/2} \rightarrow {}^4\text{I}_{13/2}$). ϕ_i represents the pump photon flux corresponding to the pump wavelengths 795 nm (ϕ_2) and 970 nm

(ϕ_4). σ_{02} and σ_{04} represent the GSA cross-sections for pumping respectively at 795 and 970 nm, while σ_b and σ_d are the cross-sections of the corresponding ESA. ρ_G and ρ_{IR} represent the resonator losses, respectively, for the laser transition in green and in infrared; their dependence on the mirrors' reflectivities (R_1 and R_2), intrinsic losses in the active medium ρ_0 , and active medium length l are given by

$$\rho = \rho_0 - \frac{1}{2l} \log(R_1 R_2). \tag{2}$$

$f_{52}\sigma_{50}$ and $f_{08}\sigma_{50}$ represent the stimulated emission, respectively the absorption cross-sections on the green laser transition, where f_{52} and f_{08} are the fractional populations of the initial, respectively final laser level of this transition. Similarly, $f_{52}\sigma_{51}$ and $f_{17}\sigma_{51}$ represent the stimulated emission, respectively absorption cross-sections on the infrared laser transition, with f_{17} the fractional population of the final laser level. k_G and k_{IR} are two factors taking into account the contribution of the spontaneous emission to the laser emission on each laser transition. The symbols v_G and v_{IR} denote the values of the speed of light at the two laser wavelengths in the active medium. The notations were kept as much as possible the same as in [13] to facilitate the comparison and corroboration of the results of the two models.

2.1. Working method

The rate equations system (1) is a dynamical system with three independent parameters, namely, the resonator losses in green (ρ_G), the resonator losses in infrared (ρ_{IR}) and the pump photon flux (ϕ_2 or ϕ_4). The information about the emission regime of the laser are obtained studying the stability of the steady-state solutions of the rate equations system (1) at various values of the three parameters. This system has attached a three-dimensional parameter space; as a scanning algorithm for the parameter space, for each value of ρ_{IR} , we scanned many values of ρ_G , for each of them finding the bifurcation values of ϕ_i .

The steady-state solutions are obtained analytically, in order to enable their use for the study of any low-concentration Er-doped crystal. In solving for the steady-state solutions, the spontaneous-emission term in the last two equations in Eqs. (1) is neglected. This term is important only for starting the laser oscillation, but is negligible in the presence of laser emission.

The results obtained from the stability analysis were verified using numerical integration of Eqs. (1) by a fourth-rank Runge–Kutta method, with the natural initial conditions (at $t = 0$, $N_i = 0$ for all $i \neq 0$ and $\varphi_G = \varphi_{IR} = 0$) and various values of the control parameters ϕ_2 , ϕ_4 , ρ_G , ρ_{IR} .

2.2. Parameters' values

The spectroscopic parameters of Er:YLF chosen for our simulations are presented in Table 1. A detailed discussion regarding their choice from the data available in the literature was given in [13].

The fractional populations of the laser levels at room temperature were calculated using the data in [18] about Er^{3+} energy levels in YLF: $f_{52} = 0.401$, $f_{08} = 0.040$, and $f_{17} = 0.083$.

The loss parameters were given values of at least 10^{-3} cm^{-1} . This minimum value corresponds, for resonator lengths between 5 cm and 1 cm, to losses through output mirror with reflectivities in the range 99%–99.8%. The presence of the losses ρ_0 in the active medium and of the losses through the rear mirror of a real laser resonator (often of the order 10^{-3} cm^{-1} themselves) usually increases the total losses over this minimum value. The maximum values of the resonator losses at the two investigated emission wavelengths were chosen to allow a good representation in parameter space of the domains corresponding to all the emission regimes possible.

Table 1
Spectroscopic parameters of Er:YLF.

| Parameter | Value | Reference |
|------------------------------------|------------------------------------|-----------|
| β_{20} | 0.613 | [19] |
| β_{21} | 0.387 | [19] |
| β_{30} | 0.001 | [19] |
| β_{31} | 0 | [19] |
| β_{32} | 0.999 | [19] |
| β_{40} | 0.087 | [19] |
| β_{41} | 0.004 | [19] |
| β_{42} | 0.006 | [19] |
| β_{43} | 0.903 | [19] |
| β_{50} | 0.488 | [19] |
| β_{51} | 0.179 | [19] |
| β_{52} | 0.015 | [19] |
| β_{53} | 0.012 | [19] |
| β_{54} | 0.306 | [19] |
| T_1 | 10000 μs | [20] |
| T_2 | 4000 μs | [20] |
| T_3 | 6.6 μs | [20] |
| T_4 | 100 μs | [20] |
| T_5 | 400 μs | [20] |
| $\sigma_{50}(551 \text{ nm})$ | $5 \times 10^{-20} \text{ cm}^2$ | [20] |
| $\sigma_{51}(850 \text{ nm})$ | $1.6 \times 10^{-19} \text{ cm}^2$ | [1] |
| $\sigma_{02}(795 \text{ nm})$ | $5 \times 10^{-21} \text{ cm}^2$ | [19] |
| $\sigma_b(795 \text{ nm})$ | 10^{-20} cm^2 | [19] |
| $\sigma_{04}(970 \text{ nm})$ | $3 \times 10^{-20} \text{ cm}^2$ | [19] |
| $\sigma_{\bar{d}}(970 \text{ nm})$ | $3 \times 10^{-20} \text{ cm}^2$ | [19] |
| $\sigma_1(551 \text{ nm})$ | $2 \times 10^{-21} \text{ cm}^2$ | [4] |

The pump flux parameters ϕ_2 and ϕ_4 were given values between $10^{16} \text{ cm}^{-2} \mu\text{s}^{-1}$ and $10^{24} \text{ cm}^{-2} \mu\text{s}^{-1}$. This large range was investigated in order to make sure that all eigenvalues of the Jacobi matrix have reached their asymptotical values and no other bifurcations are expected. This range also includes the usual experimental values of the pump flux.

The values of factors k_G and k_{IR} depend on the resonator geometry. These factors were used here only for starting the laser oscillation on each transition; therefore, their presence is important only for numerical integration of Eqs. (1) and their values can be made arbitrarily small. For the numerical integration, their values were set to $10^{-10} \text{ cm}^{-2} \mu\text{s}^{-1}$. These factors were neglected when solving for the steady-state solutions of Eqs. (1), due to their negligible contribution to the laser flux.

3. Steady-state solutions

The steady-state solutions of system (1) were obtained by setting the left-hand side of all its differential equations to 0 and solving for the populations and photon fluxes. The factors k_G and k_{IR} were neglected, and thus each of the flux equations could be factored in two. Following this factorization, there are four groups of solutions, corresponding to:

1. Emission at 850 nm: $\varphi_G = 0$ and $\varphi_{IR} \neq 0$;
2. Emission at 551 nm: $\varphi_G \neq 0$ and $\varphi_{IR} = 0$;
3. Simultaneous emission at 850 nm and 551 nm: $\varphi_G \neq 0$ and $\varphi_{IR} \neq 0$;
4. No laser emission: $\varphi_G = \varphi_{IR} = 0$.

Solutions of types 1–3 were calculated for pump at 795 nm and for pump at 970 nm. Solutions of type 4 will not be discussed here.

3.1. 795 nm pumping

The steady-state solutions of system (1) for the pump mechanism [b] (pump wavelength around 795 nm: $\phi_2 \neq 0$, $\phi_4 = 0$ in (1)) are presented below.

1. Emission at 850 nm:

$$\begin{aligned} \bar{N}_0 &= \frac{N_t + \frac{\rho_{IR}}{f_{17}\sigma_{51}}}{1 + \sigma_{02}T_{23}\phi_2} - \frac{T'_{25}}{T_5(1 + \sigma_{02}T_{23}\phi_2)} \bar{N}_5 \\ \bar{N}_1 &= \frac{f_{52}\bar{N}_5 - \frac{\rho_{IR}}{f_{17}\sigma_{51}}}{f_{17}} \\ \bar{N}_2 &= \beta_{32}\sigma_{02}T_2\phi_2\bar{N}_0 + \beta_{5432}\frac{T_2}{T_5}\bar{N}_5 \\ \bar{N}_3 &= \beta_{543}\frac{T_3}{T_5}\bar{N}_5 + \sigma_{02}T_3\phi_2\bar{N}_0 \\ \bar{N}_4 &= \beta_{54}\frac{T_4}{T_5}\bar{N}_5 \\ \bar{N}_5 &= \frac{\frac{\rho_{IR}}{f_{17}\sigma_{51}T_1} + \frac{\beta'_{321}}{T_{25}}\left(N_t + \frac{\rho_{IR}}{f_{17}\sigma_{51}}\right)}{\frac{f_{52}}{f_{17}T_1} + \frac{\beta'_{321} - \beta_{54321} + 1}{T_5}} \\ \bar{\varphi}_G &= 0 \\ \bar{\varphi}_{IR} &= \frac{1}{\rho_{IR}} \left(\frac{f_{52}}{f_{17}} \sigma_b \phi_2 - \frac{1}{T_5} \right) \bar{N}_5 - \frac{\sigma_b}{f_{17}\sigma_{51}} \phi_2. \end{aligned} \quad (3)$$

3. Emission at 551 nm: $\varphi_{IR} = 0$ added to the solution that has been found in [13] for 795 nm pumping.

4. Simultaneous emission at 850 nm and 551 nm:

$$\begin{aligned} \bar{N}_0 &= \frac{f_{52}}{f_{08}} \left(1 - \frac{\sigma_1}{\sigma_{50}f_{17}} \right) \bar{N}_5 - \frac{1}{\sigma_{50}f_{08}} \left(\rho_G - \frac{\sigma_1 \rho_{IR}}{\sigma_{51}f_{17}} \right) \\ \bar{N}_1 &= \frac{f_{52}\bar{N}_5 - \frac{\rho_{IR}}{\sigma_{51}f_{17}}}{f_{17}} \bar{N}_2 = \left[\frac{\beta_{5432}}{T_5} + \beta_{32}\frac{f_{52}}{f_{08}} \left(1 - \frac{\sigma_1}{\sigma_{50}f_{17}} \right) \sigma_{02}\phi_2 \right] \times \\ &\quad \times T_2\bar{N}_5 - \beta_{32} \left(\rho_G - \frac{\sigma_1 \rho_{IR}}{\sigma_{51}f_{17}} \right) \frac{\sigma_{02}T_2\phi_2}{\sigma_{50}f_{08}} \\ \bar{N}_3 &= \left[\frac{\beta_{543}}{T_5} + \frac{f_{52}}{f_{08}} \left(1 - \frac{\sigma_1}{\sigma_{50}f_{17}} \right) \sigma_{02}\phi_2 \right] T_3 \\ \bar{N}_5 &= \left(\rho_G - \frac{\sigma_1 \rho_{IR}}{\sigma_{51}f_{17}} \right) \frac{\sigma_{02}T_3\phi_2}{\sigma_{50}f_{08}} \\ \bar{N}_4 &= \beta_{54}\frac{T_4}{T_5}\bar{N}_5 \\ \bar{N}_5 &= \left[N_t + \frac{\rho_{IR}}{\sigma_{51}f_{17}} + \left(\rho_G - \frac{\sigma_1 \rho_{IR}}{\sigma_{51}f_{17}} \right) \frac{1 + \sigma_{02}T_{23}\phi_2}{\sigma_{50}f_{08}} \right] \\ &\quad \times \left[\frac{f_{52}}{f_{17}} + \frac{T_{25}}{T_5} + \frac{f_{52}}{f_{08}} \left(1 - \frac{\sigma_1}{\sigma_{50}f_{17}} \right) (1 + \sigma_{02}T_{23}\phi_2) \right]^{-1} \\ \bar{\varphi}_G &= \frac{1}{\sigma_1\bar{N}_1 + \rho_G} \left[\frac{-\bar{N}_1}{T_1} + \beta_{21}\frac{\bar{N}_2}{T_2} + \beta_{31}\frac{\bar{N}_3}{T_3} + \beta_{41}\frac{\bar{N}_4}{T_4} + (\beta_{51}-1)\frac{\bar{N}_5}{T_5} \right] \\ \bar{\varphi}_{IR} &= \frac{\rho_G}{\rho_{IR}(\sigma_1\bar{N}_1 + \rho_G)} \left[\left(\frac{1}{T_1} + \sigma_b\phi_2 \right) \bar{N}_1 - \beta_{21}\frac{\bar{N}_2}{T_2} - \beta_{31}\frac{\bar{N}_3}{T_3} - \beta_{41}\frac{\bar{N}_4}{T_4} - \beta_{51}\frac{\bar{N}_5}{T_5} \right] \\ &\quad - \frac{\sigma_1\bar{N}_1}{\rho_{IR}(\sigma_1\bar{N}_1 + \rho_G)} \left(\frac{\bar{N}_5}{T_5} - \sigma_b\phi_2\bar{N}_1 \right). \end{aligned} \quad (4)$$

5. The following notations have been used in Eqs. (3) and (4):

$$\begin{aligned} \beta_{543} &= \beta_{54}\beta_{43} + \beta_{53} \\ \beta_{5432} &= \beta_{543}\beta_{32} + \beta_{54}\beta_{42} + \beta_{52} \\ \beta_{54321} &= \beta_{5432}\beta_{21} + \beta_{543}\beta_{31} + \beta_{54}\beta_{41} + \beta_{51} \\ \beta_{321} &= \beta_{32}\beta_{21} + \beta_{31}\beta_{321} = \frac{\beta_{321}\sigma_{02}T_{25}\phi_2}{1 + \sigma_{02}T_{23}\phi_2} \\ T_{23} &= \beta_{32}T_2 + T_3 \\ T_{25} &= \beta_{5432}T_2 + \beta_{543}T_3 + \beta_{54}T_4 + T_5 \\ T'_{25} &= \beta_{5432}T_2 + \beta_{543}T_3 + \beta_{54}T_4 + \left(1 + \frac{f_{52}}{f_{17}} \right) T_5. \end{aligned} \quad (5)$$

3.2. 970 nm pumping

The steady-state solutions of system (1) for the pump mechanism [d] (pump wavelength 970 nm: $\phi_2 = 0, \phi_4 \neq 0$ in (1)) are given below.

1. Emission at 850 nm:

$$\begin{aligned} \bar{N}_0 &= \frac{1 + \sigma_d T_2 \phi_4}{1 + (\sigma_{04} + \sigma_d) T_2 \phi_4} \left\{ N_t + \frac{\rho_{IR}}{\sigma_{51} f_{17}} - \left[\frac{f_{52}}{f_{17}} + \frac{T_{25}(\phi_4)}{T_5} \right] \bar{N}_5 \right\} \\ \bar{N}_1 &= \frac{f_{52} \bar{N}_5 - \frac{\rho_{IR}}{\sigma_{51} f_{17}}}{f_{17}} \\ \bar{N}_2 &= \frac{\beta_{5432} T_2 \bar{N}_5 + \sigma_{04} T_2 T_5 \phi_4 \bar{N}_0}{T_5 (1 + \sigma_d T_2 \phi_4)} \\ \bar{N}_3 &= \beta_{543} \frac{T_3}{T_5} \bar{N}_5 \\ \bar{N}_4 &= \beta_{54} \frac{T_4}{T_5} \bar{N}_5 \\ \bar{\varphi}_G &= 0 \\ \bar{\varphi}_{IR} &= -\frac{\bar{N}_5}{\rho_{IR} T_5} + \frac{1}{\rho_{IR}} \sigma_d \phi_4 \bar{N}_2. \end{aligned} \tag{6}$$

2. With \bar{N}_5 the solution of a linear equation with the following coefficients (in the increasing order of the degree of \bar{N}_5):

$$\begin{aligned} a_0 &= \frac{\rho_{IR}}{\sigma_{51} f_{17}} \left[\frac{1}{T_1} + \beta_{21}(\phi_4) \sigma_{04} \phi_4 \right] \\ &\quad + \beta_{21}(\phi_4) \sigma_{04} \phi_4 N_t \\ a_1 &= \frac{f_{52}}{f_{17}} \left[\frac{1}{T_1} + \beta_{21}(\phi_4) \sigma_{04} \phi_4 \right] \\ &\quad + \frac{1}{T_5} [1 - \beta_{54321}(\phi_4) + \beta_{21}(\phi_4) \sigma_{04} T_{25}(\phi_4) \phi_4]. \end{aligned} \tag{7}$$

4. Emission at 551 nm: $\varphi_{IR} = 0$ added to the solution that has been published in [13].

5. Simultaneous emission at 850 nm and 551 nm:

$$\begin{aligned} \bar{N}_0 &= \frac{f_{52}}{f_{08} \sigma_{50}} \left(\sigma_{50} - \frac{\sigma_1}{f_{17}} \right) \bar{N}_5 - \frac{1}{f_{08} \sigma_{50}} \left(\rho_G - \frac{1}{f_{17}} \frac{\sigma_1}{\sigma_{51}} \rho_{IR} \right) \\ \bar{N}_1 &= \frac{f_{52} \bar{N}_5 - \frac{\rho_{IR}}{f_{17} \sigma_{51}}}{f_{17}} \\ \bar{N}_2 &= \beta_{5432} \frac{T_2(\phi_4)}{T_5} \bar{N}_5 + \sigma_{04} T_2(\phi_4) \phi_4 \bar{N}_0 \\ \bar{N}_3 &= \beta_{543} \frac{T_3}{T_5} \bar{N}_5 \\ \bar{N}_4 &= \beta_{54} \frac{T_4}{T_5} \bar{N}_5 \\ \bar{\varphi}_G &= \frac{1}{\sigma_1 \bar{N}_1 + \rho_G} \left[-\frac{\bar{N}_1}{T_1} + \left(\frac{\beta_{21}}{T_2} + \sigma_d \phi_4 \right) \bar{N}_2 \right. \\ &\quad \left. + \beta_{31} \frac{\bar{N}_3}{T_3} + \beta_{41} \frac{\bar{N}_4}{T_4} - \frac{1 - \beta_{51}}{T_5} \bar{N}_5 \right] \\ \bar{\varphi}_{IR} &= \frac{1}{\rho_{IR} (\rho_G + \sigma_1 \bar{N}_1)} \left[\rho_G \left(\frac{\bar{N}_1}{T_1} - \beta_{21} \frac{\bar{N}_2}{T_2} - \beta_{31} \frac{\bar{N}_3}{T_3} - \beta_{41} \frac{\bar{N}_4}{T_4} - \beta_{51} \frac{\bar{N}_5}{T_5} \right) \right. \\ &\quad \left. - \sigma_1 \bar{N}_1 \left(\frac{\bar{N}_5}{T_5} - \sigma_d \phi_4 \bar{N}_2 \right) \right]. \end{aligned} \tag{8}$$

6. with \bar{N}_5 the solution of a linear equation with coefficients (in the increasing order of the degree of \bar{N}_5):

$$\begin{aligned} b_0 &= N_t + \left[1 - \frac{\sigma_1}{f_{08} \sigma_{50}} \frac{1 + (\sigma_{04} + \sigma_d) T_2 \phi_4}{1 + \sigma_d T_2 \phi_4} \right] \times \frac{\rho_{IR}}{f_{17} \sigma_{51}} \\ &\quad + \frac{1 + (\sigma_{04} + \sigma_d) T_2 \phi_4}{1 + \sigma_d T_2 \phi_4} \frac{\rho_G}{f_{08} \sigma_{50}} \\ b_1 &= \frac{1 + (\sigma_{04} + \sigma_d) T_2 \phi_4}{1 + \sigma_d T_2 \phi_4} \frac{f_{52}}{f_{08} \sigma_{50}} \left(\sigma_{50} - \frac{\sigma_1}{f_{17}} \right) + \frac{f_{52}}{f_{17}} + \frac{T_{25}}{T_5}. \end{aligned} \tag{9}$$

Additional notations, besides those in Eqs. (5), have been used above:

$$\begin{aligned} \beta_{21}(\phi_4) &= \frac{\beta_{21} + \sigma_d T_2 \phi_4}{1 + (\sigma_{04} + \sigma_d) T_2 \phi_4} \\ \beta_{54321}(\phi_4) &= \beta_{5432} \frac{\beta_{21} + \sigma_d T_2 \phi_4}{1 + \sigma_d T_2 \phi_4} + \beta_{543} \beta_{31} \\ &\quad + \beta_{54} \beta_{41} + \beta_{51} \\ T_{25}(\phi_4) &= \beta_{5432} \frac{T_2}{1 + \sigma_d T_2 \phi_4} + \beta_{543} T_3 \\ &\quad + \beta_{54} T_4 + T_5. \end{aligned} \tag{10}$$

4. Results and discussion

4.1. 795 nm pumping

The results of the stability analysis of the steady-state solutions (3), (4) and of the solution given in [13] are synthesized in the parameter space plot in Fig. 2 for pump mechanism [b] (pump wavelength around 795 nm). This figure represents the threshold pump flux of the various emission regimes function of the resonator losses at the two laser wavelengths.

As expected, for low values of ρ_{IR} and great values of ρ_G , the laser emits in a continuous wave (CW) regime at 850 nm. The threshold of this regime does not depend on ρ_G , therefore the surface representing it could be generated by translating a curve corresponding to a certain value of ρ_G parallel to the ρ_G axis.

For sufficiently high values of ρ_{IR} , the emission at 850 nm is inhibited and the laser emits at 551 nm, with the emission regimes (CW and self-pulsing) found in [13] and the thresholds independent of ρ_{IR} . The thresholds of these regimes can be generated by the curves in Fig. 4 in [13], translated parallel to the ρ_{IR} axis.

The above-mentioned emission regimes can be identified in Fig. 3, which is a projection of the surfaces in Fig. 2 on the $\phi_2 = 0$ plane: for the domains labeled I and V the emission regimes are CW at 850 nm, respectively 551 nm, while for resonator losses in the domain labeled IV the regime can be either CW at 551 nm, or self-pulsing at 551 nm.

For the CW emission at 850 nm, the threshold pump flux could be calculated setting $\varphi_{IR} = \varphi_G = 0$ in Eqs. (1) and solving for ϕ_2 . The threshold value obtained is the solution of a second-degree equation with the following coefficients (in the increasing order of the degree):

$$\begin{aligned} c_0 &= -\frac{\rho_{IR}}{\sigma_{51} T_1} \\ c_1 &= \frac{\rho_{IR}}{\sigma_{51}} (\beta_{54321} - 1) \sigma_b \\ &\quad - \left[\frac{\rho_{IR}}{\sigma_{51}} \left(\beta_{321} + \frac{T_{23}}{T_1} \right) + \beta_{321} f_{17} N_t \right] \sigma_{02} \\ c_2 &= \left\{ [(\beta_{54321} - 1) T_{23} - \beta_{321} T_{25}] \frac{\rho_{IR}}{\sigma_{51}} \right. \\ &\quad \left. + \beta_{321} f_{52} T_5 N_t \right\} \sigma_{02} \sigma_b \end{aligned} \tag{11}$$

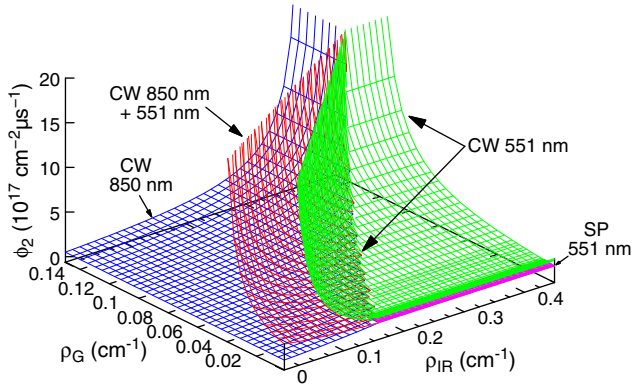


Fig. 2. Dependence of the emission thresholds for various emission regimes on ρ_{IR} and ρ_G , as obtained from the stability analysis and analytical calculations, for pump mechanism [b]. The labels denote the temporal emission regime and the emission wavelength that determine the various emission regimes. CW – continuous wave; SP – self-pulsing.

with a singularity at

$$\rho_{IR} = \frac{\beta_{321} f_{52} \sigma_{51} T_5 N_t}{\beta_{321} T_{25} - (\beta_{54321} - 1) T_{23}} = 0.403 \text{ cm}^{-1} \quad (12)$$

where the coefficient of the second-degree term becomes zero. This value of ρ_{IR} represents a vertical asymptote for the threshold of CW emission at 850 nm in Fig. 2; the CW emission threshold at 551 nm also has a vertical asymptote at $\rho_G = 0.125 \text{ cm}^{-1}$ [13]. These asymptotes border the domain labeled VI in Fig. 3; for resonator losses in this domain, laser emission is not possible.

For resonator losses in the domains II and III, the lowest threshold belongs to the emission at 850 nm. The next in magnitude is the threshold of the simultaneous CW emission at both wavelengths, and the highest threshold belongs to emission at 551 nm. The surfaces representing the thresholds of these three regimes are represented in Fig. 2; they overlap partially and they also present asymptotes. These surfaces' projections on the $\phi_2 = 0$ plane in Fig. 3 cover domains I, II and III (for the threshold of CW emission at 850 nm), II and III (for the threshold of simultaneous CW emission at both wavelengths) and III (for the threshold of the CW 551 nm emission). Therefore, for resonator losses in domain II, there are two emission regimes possible: CW at 850 nm and CW simultaneous emission at both

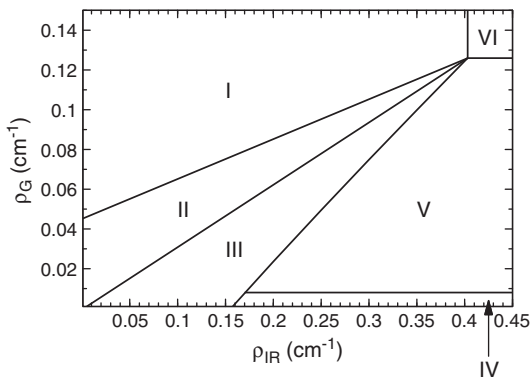


Fig. 3. Projection of the surfaces represented in Fig. 2 on the plane $\phi_2 = 0$; the numbered zones contain values of the two loss parameters corresponding to various emission regimes. I – the only possible laser emission is CW at 850 nm; II – two possible emission regimes: CW at 850 nm and CW simultaneously at 850 and 551 nm; III – three possible emission regimes: CW at 850 nm, CW simultaneously at 850 and 551 nm, and CW at 551 nm; IV – two possible emission regimes: CW at 551 nm and self-pulsed at 551 nm; V – only one emission regime possible: CW at 551 nm; VI – no laser emission possible.

wavelengths. For losses in domain III, there are three regimes possible: CW at 850 nm, CW at both wavelengths, and CW at 551 nm.

The threshold of the CW emission at both wavelengths simultaneously could be analytically calculated setting $\phi_C = 0$ in Eqs. (1) and solving for ϕ_2 ; the threshold pump flux is the solution of a linear equation with coefficients (in the increasing order of the degree):

$$\begin{aligned} d_0 &= \frac{1}{\sigma_{51} f_{17}} \left[\frac{1}{T_1} \left(\frac{T_{25}}{T_5} + \frac{f_{52}}{f_{08}} \right) - \frac{1 - \beta_{54321}}{T_5} \left(1 - \frac{\sigma_1}{\sigma_{50} f_{08}} \right) \right] \rho_{IR} \\ &\quad - \left(\frac{f_{52}}{f_{17} T_1} + \frac{1 - \beta_{54321}}{T_5} \right) \left(\frac{1}{f_{08} \sigma_{50}} + N_t \right) \\ d_1 &= \frac{\sigma_{02}}{\sigma_{51} f_{08} f_{17}} \left[\frac{\sigma_1 (1 - \beta_{54321}) T_{23} + \beta_{321} T_{25}}{\sigma_{50} T_5} + f_{52} \left(\beta_{321} + \frac{T_{23}}{T_1} \right) \right] \rho_{IR} \\ &\quad - \frac{\sigma_{02}}{f_{08} \sigma_{50}} \left[\frac{f_{52} T_{23}}{f_{17} T_1} + (1 - \beta_{54321}) \frac{T_{23}}{T_5} + \beta_{321} \left(\frac{f_{52}}{f_{17}} + \frac{T_{25}}{T_5} \right) \right] \rho_G \\ &\quad + \beta_{321} \frac{f_{52}}{f_{08}} \sigma_{02} \left(1 - \frac{1}{f_{17} \sigma_{50}} \right) N_t. \end{aligned} \quad (13)$$

The linear equation $d_1(\rho_{IR}, \rho_G) = 0$ defines a vertical asymptote for this emission threshold, asymptote projected in Fig. 3 on the boundary between domains I and II.

For the ease of visualization of the various details of the parameter space, we sliced in Fig. 2 with various planes given by constant values of ρ_{IR} . The values of ρ_{IR} were chosen so as to illustrate all types of sections and are not related to the practical possibilities of obtaining the values of the control parameters.

For $\rho_{IR} = 0.005 \text{ cm}^{-1}$, the section is presented in Fig. 4. At this value of ρ_{IR} , the possible laser emission regimes are CW emission at 850 nm and CW emission at both 850 nm and 551 nm simultaneously. The threshold of the 850 nm emission is independent of ρ_G and is the lowest.

For $\rho_{IR} = 0.05 \text{ cm}^{-1}$, the section is presented in Fig. 5. The CW 850-nm emission threshold is lowest and independent of ρ_G . It is followed by the threshold of the CW simultaneous emission at both wavelengths and by the threshold of the CW laser emission at 551 nm.

The section obtained for $\rho_{IR} = 0.12 \text{ cm}^{-1}$ is presented in Fig. 6. Fig. 7 presents a detail of Fig. 6, making visible a domain of self-pulsed emission at both laser wavelengths, at very low values of ρ_G , which could not be represented in Figs. 2 and 3. Besides this regime, there are three CW emission regimes possible: at 850 nm, at both wavelengths simultaneously, and at 551 nm.

Fig. 8 represents a section through the parameter space for $\rho_{IR} = 0.2 \text{ cm}^{-1}$. This section passes through all domains in Fig. 3 except VI: as ρ_G increases, there is first a domain of self-pulsed

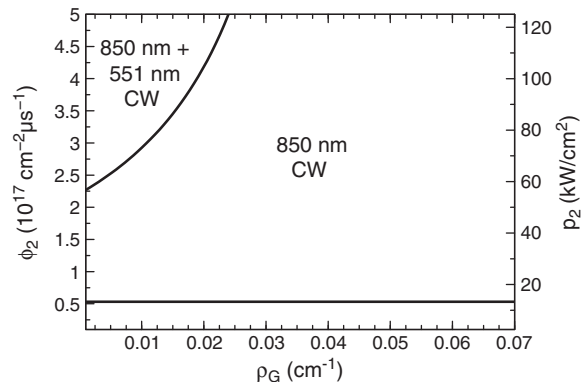


Fig. 4. Section through the parameter space of system (1) for pump mechanism [b], plane $\rho_{IR} = 0.005 \text{ cm}^{-1}$. The various domains in this plane are labeled with emission wavelength (s) and temporal emission regime (CW – continuous wave) that characterize the laser emission.

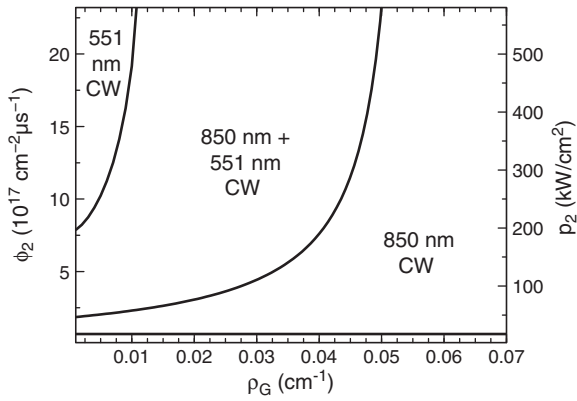


Fig. 5. Section through the parameter space of system (1) for pump mechanism [b], plane $\rho_{IR} = 0.05 \text{ cm}^{-1}$. The labeling of the domains follows the same convention as for Fig. 4.

emission at 551 nm, accompanied, at greater values of ϕ_2 , by a domain of CW emission at the same wavelength (domain IV in Fig. 3); then, there is a domain of CW 551-nm emission (domain V in Fig. 3); the next is a domain in which CW emission is possible at 850 nm or at 850 nm and 551 nm simultaneously or at 551 nm, depending on the value of ϕ_2 (domain III in Fig. 3); then, a domain in which there are two possible emission regimes: CW at 850 nm and CW at both wavelengths simultaneously (domain II in Fig. 3); and the last, a domain in which only CW emission at 850 nm is possible (domain I in Fig. 3).

The results of the stability analysis were checked by numerical integration of the rate equations (1). The numerical integration confirmed the results yielded by the stability analysis. However, for $\rho_{IR} = 0.05 \text{ cm}^{-1}$, at values of ρ_G between 0.001 cm^{-1} and 0.0025 cm^{-1} and ϕ_2 around $4 \times 10^{17} \text{ cm}^{-2} \mu\text{s}^{-1}$, oscillations were obtained in the laser emission at both wavelengths in points of the parameter space where the stability analysis predicted CW emission (see Fig. 5). These oscillations, illustrated in Fig. 9, are probably due to the fact that the initial conditions in this case are not contained in the attraction basin of the steady-state solution (4). The first to start laser oscillation in this case is the transition at 850 nm, due to its easier way of building population inversion; it presents relaxation oscillations and continues to grow after these oscillations cease. As the main part of the population accumulates on the long-lived level $^4I_{11/2}$, the ground level is depleted; meanwhile, laser emission at 850 nm causes a steeper increase of N_1 and, thus, the increase of N_5 through ESA [b]. As N_5 increases and N_0 decreases, population inversion on the transition at 551 nm reaches emission threshold. The pulsed emission at 551 nm influences the temporal evolution of the emission at 850 nm by the modulation of N_5 (directly

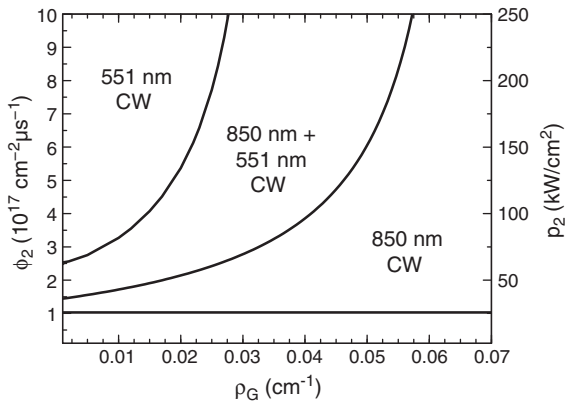


Fig. 6. Section through the parameter space of system (1) for pump mechanism [b], plane $\rho_{IR} = 0.12 \text{ cm}^{-1}$.

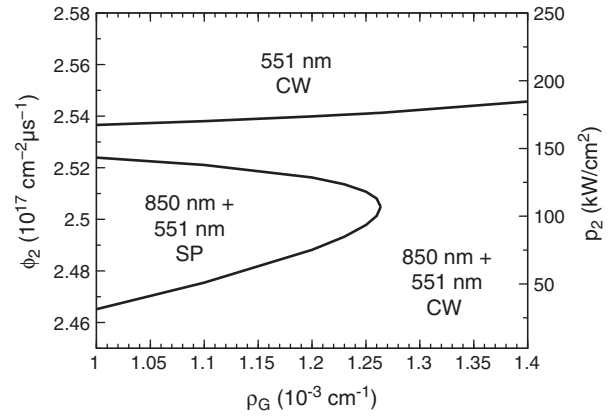


Fig. 7. Section through the parameter space of system (1) for pump mechanism [b], plane $\rho_{IR} = 0.12 \text{ cm}^{-1}$. Detail of Fig. 6. The notation SP marks the domain in this plane corresponding to a self-pulsing regime.

and N_1 (by the ESR at 551 nm, that depletes $^4I_{13/2}$). The time evolution of the populations when the system reaches a periodic regime is presented in Fig. 10: a green pulse causes the decrease of N_1 by ESR, thus creating conditions for an IR laser pulse; this latter is followed by a train of relaxation oscillations of φ_{IR} , while N_1 and N_5 slightly increase and N_0 slightly decreases, till the population inversion between $^4S_{3/2}$ and ground state reaches threshold again and the next green laser pulse perturbs again the populations. Irregular variation of the populations could be observed for some values of the three parameters (for example, $\rho_G = 1.5 \times 10^{-3} \text{ cm}^{-1}$, $\rho_{IR} = 0.05 \text{ cm}^{-1}$, $\phi_2 = 4.1 \times 10^{17} \text{ cm}^{-2} \mu\text{s}^{-1}$).

The various regimes predicted by the stability analysis for single-wavelength emission (self-pulsing and CW) were illustrated in previous works [11,13].

We illustrate in Fig. 11 the kinetics of the simultaneous CW emission at 850 nm and 551 nm, for $\rho_{IR} = 0.05 \text{ cm}^{-1}$, $\rho_G = 0.02 \text{ cm}^{-1}$, and $\phi_2 = 10^{18} \text{ cm}^{-2} \mu\text{s}^{-1}$. The temporal evolution of the populations N_0, N_1, N_2 and N_5 together with the laser photon flux φ_{IR} and φ_G is shown. The emission at 850 nm is started first, due to an easier build-up of inversion between level $^4S_{3/2}$ and $^4I_{13/2}$, initially not populated. As φ_{IR} passes through relaxation oscillations and continues to increase, the population inversion between levels $^4S_{3/2}$ and $^4I_{15/2}$ increases both by the increase of $^4S_{3/2}$ population and by the depletion of the fundamental state by the pump absorption, while the main part of the population accumulates on the long-lived level $^4I_{11/2}$. The laser emission at 551 nm starts and its relaxation oscillations cause relaxation oscillations to φ_{IR} also, until both photon fluxes settle to a CW regime. The laser emission at 551 nm starts the ESR at 551 nm, thus hindering the accumulation of population on $^4I_{13/2}$ and stabilizing the populations at values close to those reached at the

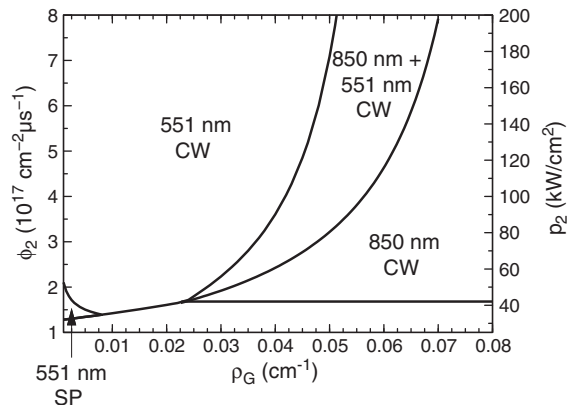


Fig. 8. Section through the parameter space of system (1) for pump mechanism [b], plane $\rho_{IR} = 0.2 \text{ cm}^{-1}$.

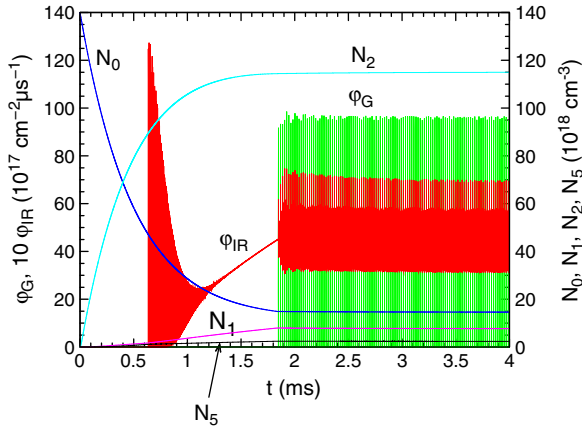


Fig. 9. Transient behavior of populations N_0, N_1, N_2, N_5 , and of the laser fluxes for $\rho_{IR} = 0.05 \text{ cm}^{-1}, \rho_G = 2.5 \times 10^{-3} \text{ cm}^{-1}, \phi_2 = 3.7 \times 10^{17} \text{ cm}^{-2} \mu\text{s}^{-1}$.

start of the green laser emission; thus, laser emission is made possible at both wavelengths simultaneously.

Another interesting regime is the self-pulsing emission at both wavelengths, which can be obtained for values of the parameters represented in Fig. 7. The evolution of the populations in this case is similar to that represented in Fig. 9. As can be noticed, all pulsed emission regimes of the Er:YLF laser are initiated by the 551-nm emission.

4.2. 970 nm pumping

For the pump mechanism [d], the results obtained from the stability analysis are presented in Fig. 12, which is a plot of the thresholds of various laser emission regimes function of the resonator losses ρ_{IR} and ρ_G . As can be seen in this figure, the laser can settle to any of four emission regimes: CW at 551 nm, CW at 850 nm, CW at both wavelengths simultaneously, and self-pulsing at both wavelengths.

Fig. 13 represents a projection on the $\phi_4 = 0$ plane of the surfaces represented in Fig. 12. The plane $\phi_4 = 0$ can be divided into seven domains, as in Fig. 13, labeled from I to VII.

For resonator losses in domain I, only CW emission at 850 nm is possible (only solution (6) is stable at values of ϕ_4 greater than the threshold represented in Fig. 12).

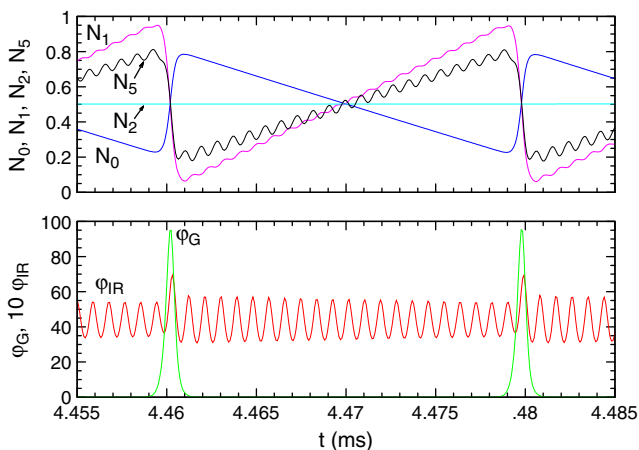


Fig. 10. Self-pulsed emission at both wavelengths, for $\rho_{IR} = 0.05 \text{ cm}^{-1}, \rho_G = 2.5 \times 10^{-3} \text{ cm}^{-1}, \phi_2 = 3.7 \times 10^{17} \text{ cm}^{-2} \mu\text{s}^{-1}$. Down: ϕ_G (units of $10^{17} \text{ cm}^{-2} \mu\text{s}^{-1}$) and ϕ_{IR} multiplied by a factor of ten (the same units). Up: populations N_0, N_1, N_2, N_5 , in arbitrary units, rescaled by a linear transform (setting each continuous component to 0.5 and rescaling N_1 to fit in the interval [0,1], while preserving their variations relative to the average).

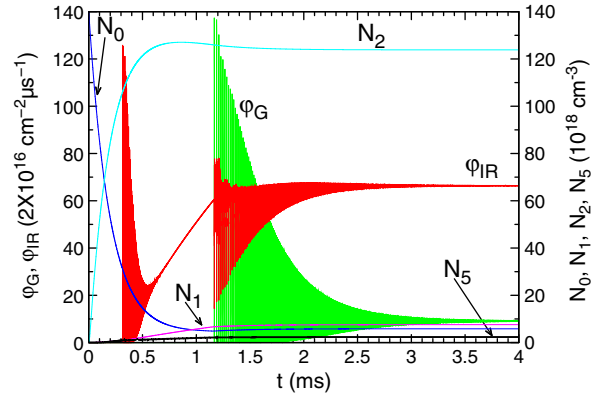


Fig. 11. Evolution to CW emission at both wavelengths simultaneously, for $\rho_{IR} = 0.05 \text{ cm}^{-1}, \rho_G = 0.02 \text{ cm}^{-1}, \phi_2 = 10^{18} \text{ cm}^{-2} \mu\text{s}^{-1}$.

The threshold for 850 nm emission could be calculated in this case setting $\phi_{IR} = \phi_G = 0$ in Eqs. (1) and solving the system for ϕ_4 . The threshold pump flux is a solution of the second-degree equation with the following coefficients (in the order of the increasing degree):

$$\begin{aligned}
 e_0 &= -\frac{\rho_{IR}}{\sigma_{51}} \\
 e_1 &= -f_{17}\beta_{21}\sigma_{04}T_1N_t \\
 &\quad -[(1-\beta_{5432})\sigma_dT_2 + (\beta_{21}T_1 + T_2)\sigma_{04}] \\
 e_2 &= \sigma_{04}\sigma_dT_2 \left[(f_{52}T_5 - f_{17}\beta_{5431}T_1)N_t - \frac{\rho_{IR}}{\sigma_{51}}T_{15_2} \right]
 \end{aligned}
 \tag{14}$$

where the following notations have been added to the ones made above:

$$\begin{aligned}
 \beta_{5431} &= \beta_{543}\beta_{31} + \beta_{54}\beta_{41} + \beta_{51} \\
 T_{15_2} &= \beta_{5431}T_1 + \beta_{543}T_3 + \beta_{54}T_4 + T_5.
 \end{aligned}
 \tag{15}$$

The threshold pump flux has a singularity at

$$\rho_{IR} = \frac{f_{52}T_5 - f_{17}\beta_{5431}T_1}{T_{15_2}} \sigma_{51}N_t = 0.115 \text{ cm}^{-1}
 \tag{16}$$

where the coefficient of the second-degree term becomes zero. This value of ρ_{IR} defines a vertical asymptote for the CW threshold of 850 nm emission (a vertical plane parallel to the ρ_G axis).

For losses in domain IV, there is only one emission regime possible: CW emission at both wavelengths simultaneously (only solution (8) is

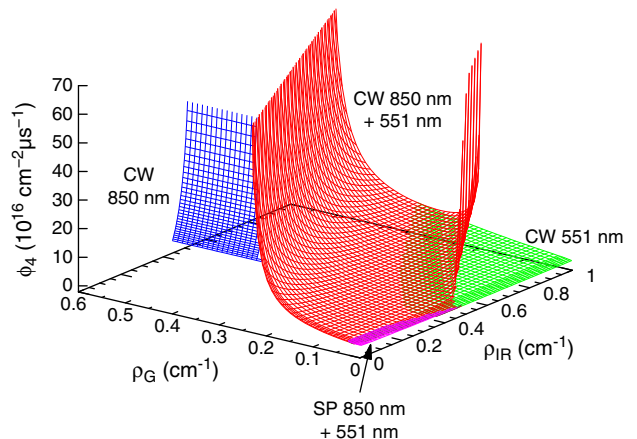


Fig. 12. Dependence of the thresholds of various emission regimes on the resonator losses ρ_{IR} and ρ_G for the Er:YLF laser pumped at 970 nm.

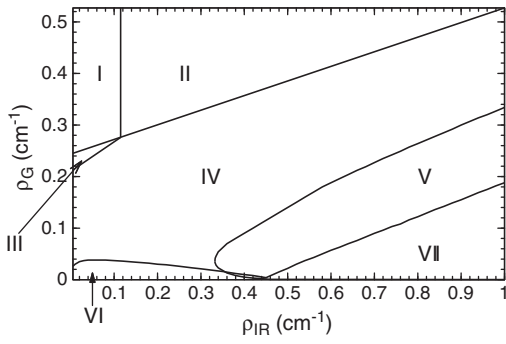


Fig. 13. Projection of the surfaces represented in Fig. 12 on the $\phi_4=0$ plane. I – domain of CW emission at 850 nm; II – no laser emission possible; III – two emission regimes possible: CW emission at 850 nm and CW emission at both wavelengths simultaneously; IV – domain of CW emission at both wavelengths simultaneously; V – two emission regimes possible: CW at 551 nm and CW at both wavelengths; VI – self-pulsed emission at both wavelengths; VII – CW emission at 551 nm.

stable for sufficiently great values of ϕ_4). Domains I and IV are overlapped (their intersection being marked with III in Fig. 13), as the surface representing CW emission at both wavelengths is superposed over the CW 850-nm emission threshold (see Fig. 12); for values of losses in their intersection, both CW emission at 850 nm and CW emission at both wavelengths are possible, with thresholds represented in Fig. 12.

For domain II (bounded by the vertical asymptote of the CW 850-nm threshold and the vertical asymptote of the simultaneous CW emission threshold), both losses are too large to allow laser emission (all steady-state solutions are unstable, regardless of the pump flux).

Domain V represents the overlapping of the projections of two surfaces (see Fig. 12): one representing the threshold of CW emission at both wavelengths, the other representing the threshold of CW emission at 551 nm. Therefore, both these regimes can be obtained in this domain, depending on the values of the pump flux.

For losses in domain VI, there are two possible emission regimes: CW emission at both wavelengths and self-pulsed emission at both wavelengths. The only solution that can become stable in this domain is (8); this solution also presents two Hopf bifurcations (considering fixed losses and the only control parameter remaining ϕ_4): one leading to its instability, and one that leads to stability again. For values of ϕ_4 between these two bifurcation values, the emission regime is self-pulsing.

A slight superposition of domains V and VI can be observed in Fig. 13. For values of losses in this intersection of the two domains, emission at both wavelengths (self-pulsed or CW) as well as emission at 551 nm can be obtained with different values for their thresholds.

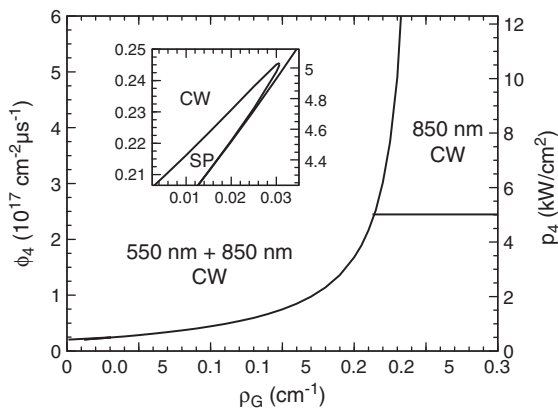


Fig. 14. Section through the parameter space of system (1) for pump mechanism [d], plane $\rho_{IR}=0.01\text{ cm}^{-1}$. Inset: detail of this section at low values of ρ_G and ϕ_4 ; CW – continuous-wave emission at both wavelengths; SP – self-pulsing at both wavelengths.

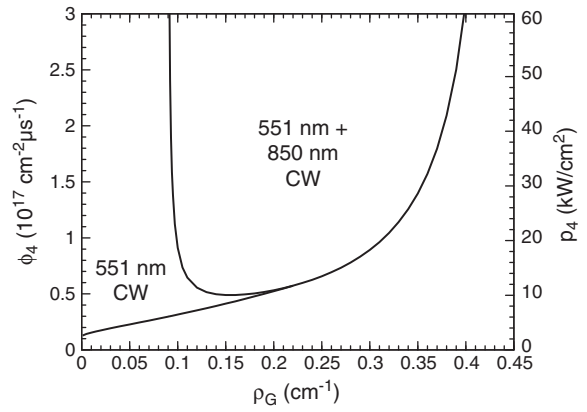


Fig. 15. Section through the parameter space of system (1) for pump mechanism [d], plane $\rho_{IR}=0.7\text{ cm}^{-1}$.

In domain VII, only emission at 551 nm is possible (the only solution that can become stable at sufficiently great values of ϕ_4 is the solution found in [13] for 551 nm). The dynamics of the laser emission for losses placed in this domain is the same as that described in [13], regardless the values of ρ_{IR} .

For a better visualization of the parameter space mapping in domain VI, a section of the surfaces represented in Fig. 12 by the vertical plane $\rho_{IR}=0.005\text{ cm}^{-1}$, which passes through domains VI and I, is presented in Fig. 14. For $\rho_G < 0.026\text{ cm}^{-1}$, at low values of ϕ_4 there is a short range of ϕ_4 values for which emission is CW at both wavelengths; as ϕ_4 increases, a Hopf bifurcation value of ϕ_4 follows that leads to instability of solution (8), opening a range of values corresponding to self-pulsing emission at both laser wavelengths. As ϕ_4 further increases, solution (8) regains its stability by another Hopf bifurcation and the laser settles again to CW emission at both 551 nm and 850 nm. This behavior can be more clearly seen in the inset in Fig. 14. For $0.026\text{ cm}^{-1} < \rho_G < 0.213\text{ cm}^{-1}$, there is only one emission regime possible – CW at both wavelengths – as there is only solution (8) that can become stable. For still greater values of ρ_G , emission is possible at 850 nm CW (lowest threshold) and at both wavelengths CW, until the threshold of the CW emission at both wavelengths tends to infinity; for values of ρ_G greater than the vertical asymptote of this threshold, only CW emission at 850 nm is possible.

Fig. 15 presents a section through the surfaces represented in Fig. 12, by the plane $\rho_{IR}=0.7\text{ cm}^{-1}$. This plane passes through domains VII, V, IV, and II in Fig. 13. In this section, the change of emission regime as ρ_G increases is visible: at low values of ρ_G , only CW emission in green is possible (domain VII); then, the threshold of CW emission at both wavelengths decreases and this regime becomes also available (domain V), and for ρ_G greater than about 0.22 cm^{-1} CW

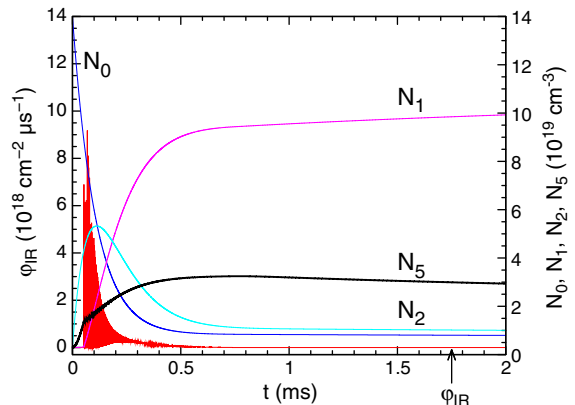


Fig. 16. Self-saturated emission at 850 nm, for $\rho_{IR}=0.7\text{ cm}^{-1}$, $\rho_G=0.45\text{ cm}^{-1}$, and $\phi_4=3 \times 10^{17}\text{ cm}^{-2}\mu\text{ s}^{-1}$.

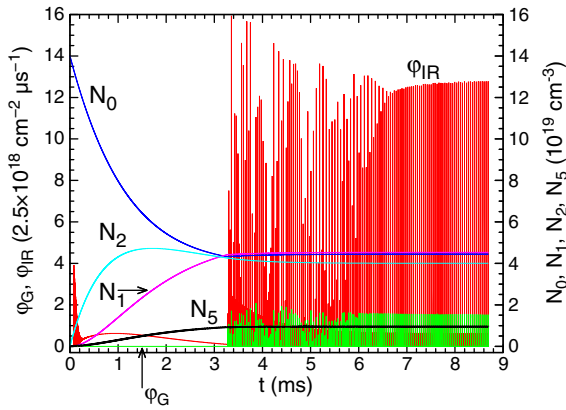


Fig. 17. Self-pulsed emission at both wavelengths, for $\rho_{IR}=0.01 \text{ cm}^{-1}$, $\rho_G=0.01 \text{ cm}^{-1}$, and $\phi_4=2.1 \times 10^{16} \text{ cm}^{-2} \mu\text{s}^{-1}$.

emission at 551 nm and 850 nm becomes the only emission regime possible (domain IV), until its threshold tends to infinity and laser emission is no longer possible (domain II).

The results obtained by the stability analysis were verified using numerical integration of Eqs. (1). The results of the numerical integration confirmed the asymptotic behavior predicted by stability analysis and also put into evidence transient effects. For example, for $\rho_{IR}=0.7 \text{ cm}^{-1}$, $\rho_G=0.45 \text{ cm}^{-1}$ and $\phi_4=3 \times 10^{17} \text{ cm}^{-2} \mu\text{s}^{-1}$, a self-saturated emission at 850 nm was observed (Fig. 16), although the asymptotic behavior of the laser is that predicted by the stability analysis (that is, no laser emission – see Fig. 15). In this regime, the emission at 850 nm is started, but ceases due to the population accumulation on the long-lived final laser level $^4I_{13/2}$.

The self-pulsing regime can be found for values of parameters represented in the inset of Fig. 14. The results obtained for one set of parameters in this domain ($\rho_{IR}=0.01 \text{ cm}^{-1}$, $\rho_G=0.01 \text{ cm}^{-1}$, and $\phi_4=2.1 \times 10^{16} \text{ cm}^{-2} \mu\text{s}^{-1}$) are represented in Fig. 17. As can be easily seen, the laser emission at 850 nm is started first; after relaxation oscillations during a few hundred microseconds, the laser photon flux reaches a maximum value and then decreases, due to the accumulation of population (N_1) on the final laser level. Its decrease is interrupted by the start of the emission at 551 nm when the ground state is sufficiently depleted to raise the inversion above threshold. The start of laser emission on this transition provides another mechanism for the depletion of $^4I_{13/2}$, namely the ESR.

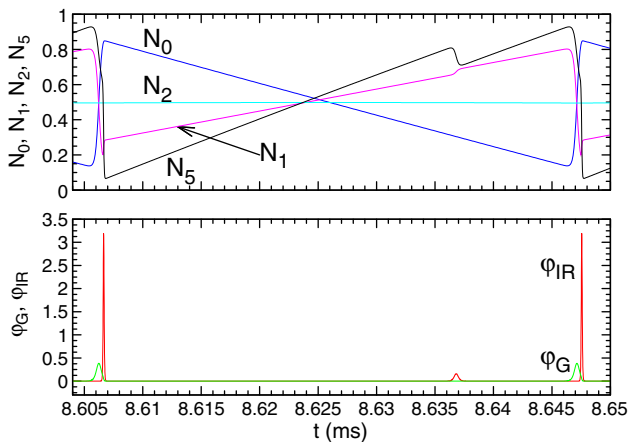


Fig. 18. Self-pulsed emission at both wavelengths, for $\rho_{IR}=0.01 \text{ cm}^{-1}$, $\rho_G=0.01 \text{ cm}^{-1}$, and $\phi_4=2.1 \times 10^{16} \text{ cm}^{-2} \mu\text{s}^{-1}$. Down: ϕ_{IR} and ϕ_G , in units of $10^{19} \text{ cm}^{-2} \mu\text{s}^{-1}$. Up: populations N_0, N_1, N_2, N_5 , in arbitrary units, rescaled by a linear transform (setting each continuous component to 0.5 and rescaling N_1 to fit in the interval [0,1], while preserving their variations relative to the average).

The evolution of the populations when the laser reaches a periodic behavior is presented in Fig. 18. First, N_0 and N_1 present a slow decrease, respectively increase, while N_5 increases with a greater slope. After about 30 μs , the population inversion between levels $^4S_{3/2}$ and $^4I_{13/2}$ reaches threshold and a low-intensity laser pulse is emitted at 850 nm. This pulse lowers the population inversion to a value under the emission threshold at 850 nm. After about 10 μs , the population inversion between $^4S_{3/2}$ and $^4I_{15/2}$ reaches threshold value and a laser pulse is emitted at 551 nm. This pulse causes a sudden decrease of N_1 due to the ESR process and thus makes possible the emission of a more intense pulse at 850 nm. This pulse depletes $^4S_{3/2}$ and increases the population of $^4I_{13/2}$, lowering the population inversion between these levels under its threshold value and increasing the reabsorption losses in green from $^4I_{13/2}$, thus stopping laser emission on both transitions. After this pulse, the cycle begins again.

The CW emission at both wavelengths simultaneously can be obtained for $\rho_{IR}=0.01 \text{ cm}^{-1}$, $\rho_G=0.05 \text{ cm}^{-1}$, and $\phi_4=10^{17} \text{ cm}^{-2} \mu\text{s}^{-1}$ (see Fig. 14). The evolution in time of populations and laser photon flux for these parameter values is represented in Fig. 19. The laser emission is started first on the transition $^4S_{3/2} \rightarrow ^4I_{13/2}$, that benefits of an easier way to raise a population inversion in its four-level scheme. The start of this laser emission accelerates the increase of population N_1 on the final laser level, and this finally leads to a decrease of the laser flux ϕ_{IR} . Simultaneously, the ground level is depleted by the pump mechanism and population is accumulated on the long-lived level $^4I_{11/2}$. The population inversion on transition $^4S_{3/2} \rightarrow ^4I_{15/2}$ increases due to both the increase of N_5 and the depletion of the ground level $^4I_{15/2}$, till it reaches the emission threshold and laser emission at 551 nm is started. This process starts the ESR process at 551 nm, thus hindering the accumulation of population on $^4I_{13/2}$ and stabilizing the populations at values where the emission at 850 nm is still possible. After the oscillation relaxations, both ϕ_{IR} and ϕ_G find their non-zero steady-state values.

4.3. Discussion

For pump mechanism [b], CW emission at a single wavelength can be obtained by setting the resonator losses in the convenient domain in Fig. 3. For CW emission at 850 nm, losses in domain I are required. For CW emission at 551 nm, the losses must be either in domain V or in domain III, at values of ϕ_2 greater than the thresholds represented in Fig. 2; CW emission has a lower threshold for losses in domain V than in domain III, the latter being characterized by larger rapidly-increasing values. CW emission at both wavelengths simultaneously can be obtained for losses in domain II; however, this possibility exists only for a limited range of values of the pump flux (limited at one end by the threshold of the CW emission at both wavelengths and at the other by the threshold of the CW emission at 551 nm). For these

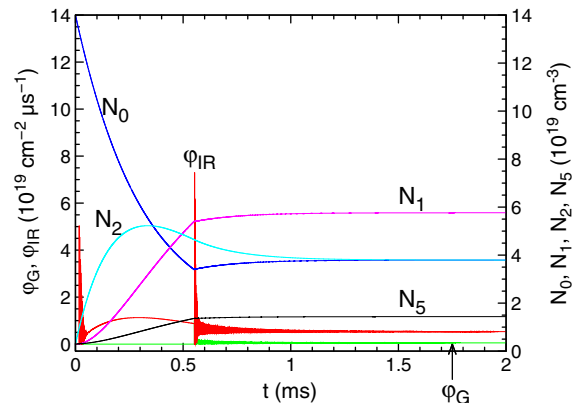


Fig. 19. Evolution to CW emission at both wavelengths simultaneously, for $\rho_{IR}=0.01 \text{ cm}^{-1}$, $\rho_G=0.05 \text{ cm}^{-1}$, and $\phi_4=10^{17} \text{ cm}^{-2} \mu\text{s}^{-1}$.

reasons, this pump mechanism is less fitted for the achievement of CW emission at both wavelengths.

Pump mechanism [d] does not favor CW emission at 850 nm alone, which is allowed with a threshold greater than that calculated for pump mechanism [b]. Its threshold also presents a more rapid increase with ρ_{IR} than in the case of 795-nm pumping. This fact can be explained by the presence, for pump mechanism [b], of a supplementary mechanism that depletes the $^4I_{13/2}$ level and facilitates laser emission at 850 nm: the ESA $^4I_{13/2} \rightarrow ^2H_{11/2}$.

For pump mechanism [d], the broadest domain in the parameter space is allocated to the CW emission at 850 nm and 551 nm simultaneously. This regime is characterized by a lower threshold in this pump scheme than in the pump scheme [b]. The threshold in this case can reach values as low as $2 \times 10^{16} \text{ cm}^{-2} \mu\text{s}^{-1}$ (for $\rho_{IR} = 0.3 \text{ cm}^{-1}$, $\rho_G = 0.034 \text{ cm}^{-1}$), while for 795-nm pumping, the minimum threshold of the same regime is about one order of magnitude greater (for $\rho_{IR} = 0.12 \text{ cm}^{-1}$, $\rho_G = 0.01 \text{ cm}^{-1}$; see Fig. 6). For pumping at 970 nm, simultaneous emission at both wavelengths is also the only regime that presents self-pulsing, at low values of ρ_G .

CW emission at the single wavelength of 551 nm is also possible for pumping at 970 nm; its domain in the parameter space is limited at domain VI (without upper limit for ϕ_4) and domain IV (in this domain, ϕ_4 is limited upwards by the threshold of the CW emission at both wavelengths).

For practical purposes, the most interesting emission regimes for this laser are CW single wavelength (551 nm or 850 nm) and CW dual-wavelength emission. The CW emission at 551 nm was discussed in a previous work [13]; its threshold was determined as a function of ρ_G for various pump mechanisms, and Figs. 3 and 13 can help identify the values of ρ_{IR} for which this emission is possible. For pumping at 795 nm, another domain in parameter space where CW emission at 551 nm is possible was identified here (domain III in Fig. 3). However, the emission threshold in this domain is greater than in domain V (see, again, Fig. 3) and increases more rapidly.

For the CW emission at 850 nm, the most favorable of the two pump wavelengths is 795 nm, due to the second step of the pump mechanism that depletes the final laser level and contributes to maintaining the population inversion on this transition. In fact, for every ion excited from $^4I_{13/2}$ to $^4S_{3/2}$, the population inversion increases with two units, while for the pump at 970 nm an ion excited to $^4S_{3/2}$ means a net gain of only one unit in population inversion. For pumping at 795 nm, this emission regime is accessible for example, for $\rho_{IR} = 0.05 \text{ cm}^{-1}$, $\rho_G = 0.1 \text{ cm}^{-1}$, and $\phi_2 > 6.9 \times 10^{16} \text{ cm}^{-2} \mu\text{s}^{-1}$ (see Fig. 5). These parameters can be obtained experimentally in a monolithic Er(1 at.%):YLF laser of 1 cm length with 100% reflectivity at 850 nm and 551 nm for the rear mirror and a reflectivity of 90.5% at 850 nm and 82% at 551 nm for the output mirror, pumped at 795 nm with a power density of at least 17.3 kW/cm^2 (that is, 5.42 W pump power focused in a spot of 200 μm diameter). The reflectivity of the output mirror was calculated neglecting the losses in the active medium; in practice, it should be adjusted for the particular value of these losses.

For the dual-wavelength CW emission, the lowest emission threshold is obtained for pumping at 970 nm. This pump mechanism is more favorable for the laser emission at 551 nm, while hampering the emission at 850 nm by the accumulation of population on the final laser level $^4I_{13/2}$. As the emission cross-section of transition $^4S_{3/2} \rightarrow ^4I_{13/2}$ is about three times greater than the emission cross-section of transition $^4S_{3/2} \rightarrow ^4I_{15/2}$, the pump mechanism [d] helps balancing the two laser transitions and this explains the much lower threshold values obtained for dual-wavelength emission when pumping at 970 nm. For this pump mechanism, CW dual-wavelength emission can be obtained, for example, for $\rho_{IR} = 0.3 \text{ cm}^{-1}$, $\rho_G = 0.034 \text{ cm}^{-1}$ and $\phi_4 > 2 \times 10^{16} \text{ cm}^{-2}$. The values of the parameters correspond to a monolithic Er (1 at.%):YLF laser of 1 cm length with 100% reflectivity at 850 nm and 551 nm for the

rear mirror and a reflectivity of 54.9% at 850 nm and 93.4% at 551 nm for the output mirror, pumped at 970 nm with a power density greater than 4.1 kW/cm^2 (that is, 1.3 W pump power focused in a spot of 200 μm diameter). The reflectivities of the output mirror were calculated with the same assumption as above, and needs to be adjusted for the particular value of the resonator losses.

5. Conclusions

A model based on rate equations, including laser emission at two wavelengths (850 nm and 551 nm), was used to predict the emission regimes (temporal behavior and wavelength(s)) of an upconversion CW-pumped Er:YLiF₄ laser. Two pump wavelengths were investigated: 795 nm and 970 nm.

For both pump mechanisms, emission is possible at 551 nm or at 850 nm or at both these wavelengths simultaneously. Regarding the temporal behavior, CW laser emission is possible in all wavelength combinations, for both pump mechanisms. Besides, self-pulsing is possible; for pump wavelength 795 nm, self-pulsing is possible both at 551 nm and at 850 nm and 551 nm mixed; for pump wavelength 970 nm, self-pulsing is possible only for laser emission at both wavelengths. Self-saturated emission is also possible as a transient, but this emission was not studied here mainly because of the time-consuming numerical calculations required for searching it in the three-dimensional parameter space.

A mapping of the parameter space was obtained showing the values of the control parameters (resonator losses in green ρ_G and infrared ρ_{IR} , and pump photon flux ϕ_2 or ϕ_4) that lead to various emission regimes at various emission wavelengths. The dependence of the thresholds of the various emission regimes on the loss parameters was also put into evidence.

The predictions obtained by stability analysis of the steady-state solutions were verified using numerical integration of the rate equations. The results of the numerical integration confirmed the predictions of the stability analysis.

Acknowledgements

This work supports the project 12135/2008 of the Romanian National Center for Management of Programs (CNMP).

References

- [1] P.E.-A. Möbert, E. Heumann, G. Huber, B.H.T. Chai, Appl. Phys. Lett. 73 (1998) 139.
- [2] T.J. Whitley, C.A. Millar, R. Wyatt, M.C. Brierley, D. Szebesta, Electron. Lett. 27 (1991) 1785.
- [3] R. Brede, E. Heumann, J. Koetke, T. Danger, G. Huber, B. Chai, Appl. Phys. Lett. 63 (1993) 2030.
- [4] T. Danger, J. Koetke, R. Brede, E. Heumann, G. Huber, B.H.T. Chai, J. Appl. Phys. 76 (1994) 1413.
- [5] J.L. He, J. Liao, H. Liu, J. Du, F. Xu, H.T. Wang, S.N. Zhu, Y.Y. Zhu, N. Ming, Appl. Phys. Lett. 83 (2003) 228.
- [6] Y.E. Hou, Y.X. Fan, J.L. He, H.T. Wang, Opt. Commun. 265 (2006) 301.
- [7] M.L. Rico, J.L. Valdés, J. Martínez-Pastor, J. Capmany, Opt. Commun. 282 (2009) 1619.
- [8] N. Pavel, Laser Phys. 20 (2010) 215.
- [9] G. Qin, S. Huang, Y. Feng, A. Shirakawa, K.-I. Ueda, IEEE Photonics Technol. Lett. 17 (2005) 1818.
- [10] G. Androz, D. Faucher, D. Gingras, R. Vallée, J. Opt. Soc. Am. B 24 (2007) 2907.
- [11] O. Toma, S. Georgescu, J. Opt. Soc. Am. B 21 (2004) 1630.
- [12] O. Toma, S. Georgescu, IEEE J. Quantum Electron. 42 (2006) 192.
- [13] O. Toma, IEEE J. Quantum Electron. 43 (2007) 519.
- [14] S.A. Pollack, D.B. Chang, M. Birnbaum, Appl. Phys. Lett. 54 (1989) 869A.
- [15] P. Xie, S.C. Rand, Appl. Phys. Lett. 57 (1990) 1182.
- [16] P. Xie, S.C. Rand, Appl. Phys. Lett. 60 (1992) 3084.
- [17] C.A. Millar, M.C. Brierley, M.H. Hunt, S.F. Carter, Electron. Lett. 26 (1990) 1871.
- [18] M.A.C. dos Santos, E. Antic-Fidancev, J.Y. Gesland, J.C. Kruppa, M. Lemaitre-Blaise, P. Porcher, J. Alloys Comp. 275–277 (1998) 435.
- [19] M. Pollnau, T. Graf, J.E. Balmer, W. Lüthy, H.P. Weber, Phys. Rev. A 49 (1994) 3990.
- [20] M. Pollnau, W. Lüthy, H.P. Weber, J. Appl. Phys. 77 (1995) 6128.